Annu. Rev. Mater. Sci. 1999. 29:261–93

HEAT CONDUCTION IN NOVEL ELECTRONIC FILMS

Kenneth E. Goodson and Y. Sungtaek Ju
Thermosciences Division, Mechanical Engineering Department, Stanford University, Stanford, California 94305; e-mail: goodson@vk.stanford.edu

KEY WORDS: silicon-on-insulator (SOI) films, superlattices, CVD diamond, high-temperature superconductors, organic films, polymer films, silicon dioxide films, thermal conductivity, heat capacity, phonon transport, electronic devices

ABSTRACT

Heat conduction in novel electronic films influences the performance and reliability of micromachined transistors, lasers, sensors, and actuators. This article reviews experimental and theoretical research on heat conduction in single-crystal semiconducting and superconducting films and superlattices, polycrystalline diamond films, and highly disordered organic and oxide films. The thermal properties of these films can differ dramatically from those of bulk samples owing to the dependence of the material structure and purity on film processing conditions and to the scattering of heat carriers at material boundaries. Predictions and data show that phonon scattering and transmission at boundaries strongly influence the thermal conductivities of single-crystal films and superlattices, although more work is needed to resolve the importance of strain-induced lattice defects. For polycrystalline films, phonon scattering on grain boundaries and associated defects causes the thermal conductivity to be strongly anisotropic and nonhomogeneous. For highly disordered films, preliminary studies have illustrated the influences of impurities on the volumetric heat capacity and, for the case of organic films, molecular orientation on the conductivity anisotropy. More work on disordered films needs to resolve the interplay among atomic-scale disorder, porosity, partial crystallinity, and molecular orientation.

INTRODUCTION

Heat conduction in thin solid films influences the performance and reliability of micromachined transistors, solid-state lasers, sensors, and actuators. Many

0084-6600/99/0801-0261$08.00

of these devices are made using conventional bulk silicon and gallium-arsenide processing technology, which patterns metal, polysilicon, and oxide films on relatively thick substrates. However, a number of relatively unconventional films and superlattices are attractive for devices because they offer enhanced electrical, optical, thermal, or thermoelectric properties. Table 1 lists examples of unconventional electronic thin films, which range in microstructure from single- and polycrystalline to fully amorphous. Examples of these novel electronic films and associated devices are shown in Figure 1.

Novel electronic films pose special complications for the study of thermal conduction. The thermal conductivities of novel thin films evolve as their processing technology matures. In polycrystalline films, such as the chemical-vapor-deposited diamond layer in Figure 1*a*, the grain size and orientation depend on the details of the nucleation and growth processes. Processing influences the thermal conductivities and volumetric heat capacities of passivation materials for integrated circuits, in particular those that aim to reduce

Table 1 Examples of novel dielectric films for electronic applications

Material structure and type	Examples	Applications
Single crystalline		
Monolayers	Ultra-thin silicon-on-insulator (SOI) films	Low-power circuits High-voltage devices Data storage cantilevers
	GaN	High-voltage devices
	SiC	Optoelectronic devices
	$YBa_2Cu_3O_7$ $BiSr_2Ca_1Cu_2O_8$	Bolometers, low-loss interconnects
Superlattices	GaAs/A1GaAs	Lasers
	InAs/A1As Si/Ge	High-mobility transistors
	BiTe/SbTe	Quantum thermoelectric devices
Poly crystalline	Diamond	High-thermal-conductivity passivation for power circuits
	Cubic BN, SiC	Power semiconductor devices
Highly disordered		
Oxides	SiOF, HSQ	Passivation for fast logic circuits
Organic materials	Alq3, TPD, PPV	Light-emitting diodes, lasers
	MEHPPV parylene, teflon	Passivation
Porous materials	Porous silicon	Adsorption sensors Optoelectronic devices
	Nanoporous silica (xerogel, aerogel)	Circuit passivation

interconnect delay through a lower dielectric constant. The importance of passivation thermal properties is illustrated by the metal-silicon contact in Figure 1*b*, where the temperature rise during rapid current transients is strongly influenced by heat diffusion into the bounding silicon dioxide. Process details also govern the defect and impurity concentrations in single-crystal strained superlattices such as the BiTe/SbTe superlattice in Figure 1*c*. Another complication is that the small dimensions of many novel films and superlattices cause heat conduction to be influenced by non-continuum interfacial phenomena, for which the appropriate governing equations and boundary conditions remain the subject of research. This is a concern for the superlattice in Figure 1*c*, as well as for the silicon-on-insulator (SOI) films in the high-voltage transistor in Figure 1*d* and in the thermomechanical data-storage cantilever in Figure 1*e*.

Although some of the novel electronic materials in Table 1 can be produced and thermally characterized in bulk form, in thin-film form their thermal properties can be dramatically different. The in-plane thermal conductivity along the film, k_a, can differ substantially from the out-of-plane conductivity normal to the film, k_n, even for materials that are isotropic in bulk form. For single-crystal semiconducting materials, the difference between bulk and film properties results in part from interfacial effects. Heat conduction is influenced by phonon scattering on film boundaries (11, 12) and, in extremely thin films, by phonon interference (13) or the modification of phonon dispersion relationships and anharmonic interaction rates (14–16). Phonon-interface scattering is responsible for the conductivity reduction illustrated in Figure 2*a* for single-crystal silicon films (17, 18). Although the boundary scattering is most prominent at low temperatures, recent room-temperature data and modeling strongly indicate that boundary scattering reduces the conductivity by 50% in films thinner than 100 nm (19).

Discrepancies between bulk and film thermal properties are also caused by structural imperfections and impurities introduced during the film growth process. For example, Figure 2*b* shows that the conductivities in polycrystalline diamond films are influenced by the grain size and orientation. The thermal conductivity is strongly anisotropic and dependent on film thickness (20, 21). Phonons scatter more frequently near grain boundaries, whose partial orientation favors conduction normal to the film (3, 4). The orientation, minimum size, and spatial growth rate of grains within the film are governed by the details of the diamond deposition process, in particular the nucleation method and the temperature and composition of the process gases.

Process-dependent material structure and stoichiometry influence the thermal conductivities and volumetric heat capacities of highly disordered films, including those of amorphous glasses and organic materials. The best representative data available at present are for conventional silicon-dioxide and

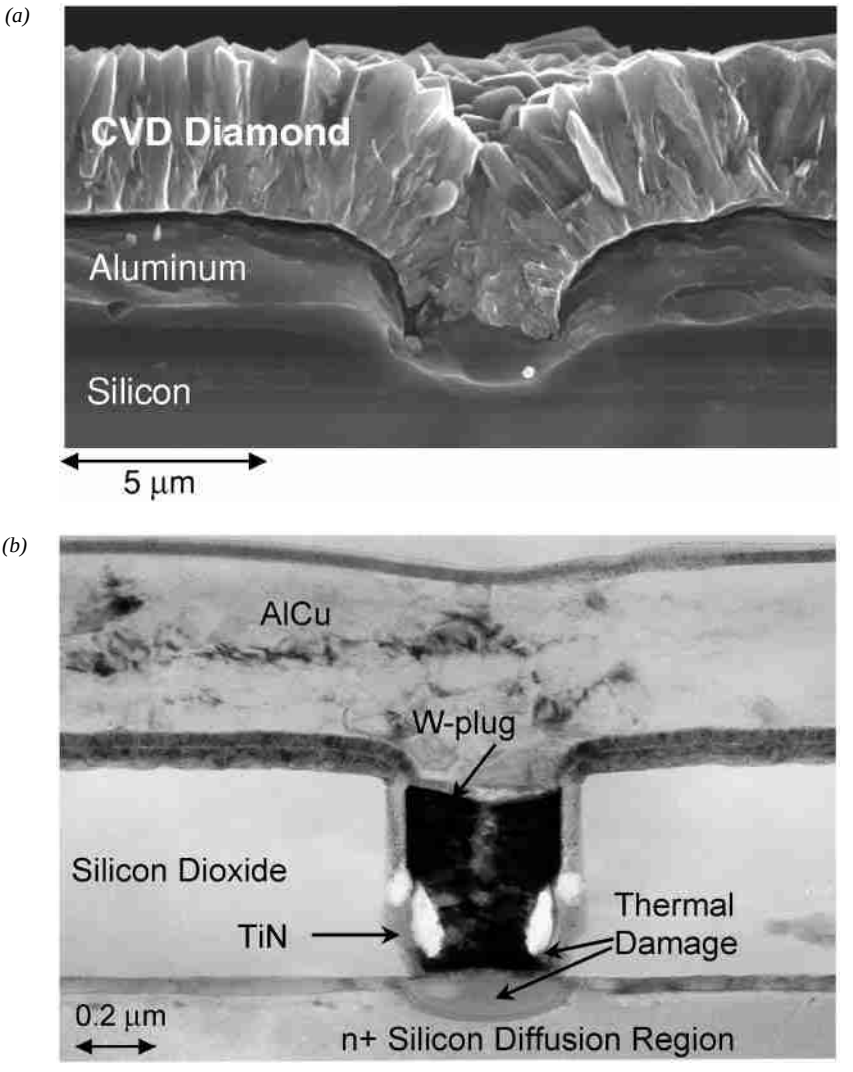

Figure 1 Electron micrographs of novel electronic films and devices: (*a*) Diamond passivation film on aluminum (1; H Güttler, DaimlerChrysler, private communication). Diamond films are promising for enhanced heat removal from power integrated circuits and for fast thermal sensors (3, 4). (*b*) Transmission electron micrograph of a VLSI metal-silicon contact, which has failed during a current pulse of sub-microsecond duration (5). The temperature rise is strongly influenced by the properties of the surrounding passive material. (*c*) Transmission electron micrograph of a BiTe/SbTe superlattice (6), which is targeted for high-performance solid-state cooling (7). (*d*) High-voltage lateral transistor containing a single-crystal silicon-on-insulator (SOI) layer (8). Lateral heat conduction in the silicon layer, which has been fabricated as thin as 200 nm, governs device cooling (9). (*e*) Single-crystal silicon cantilever and tip for high-density thermomechanical data storage. Thermal conduction governs the frequency with which bits may be carved into an organic substrate (10).

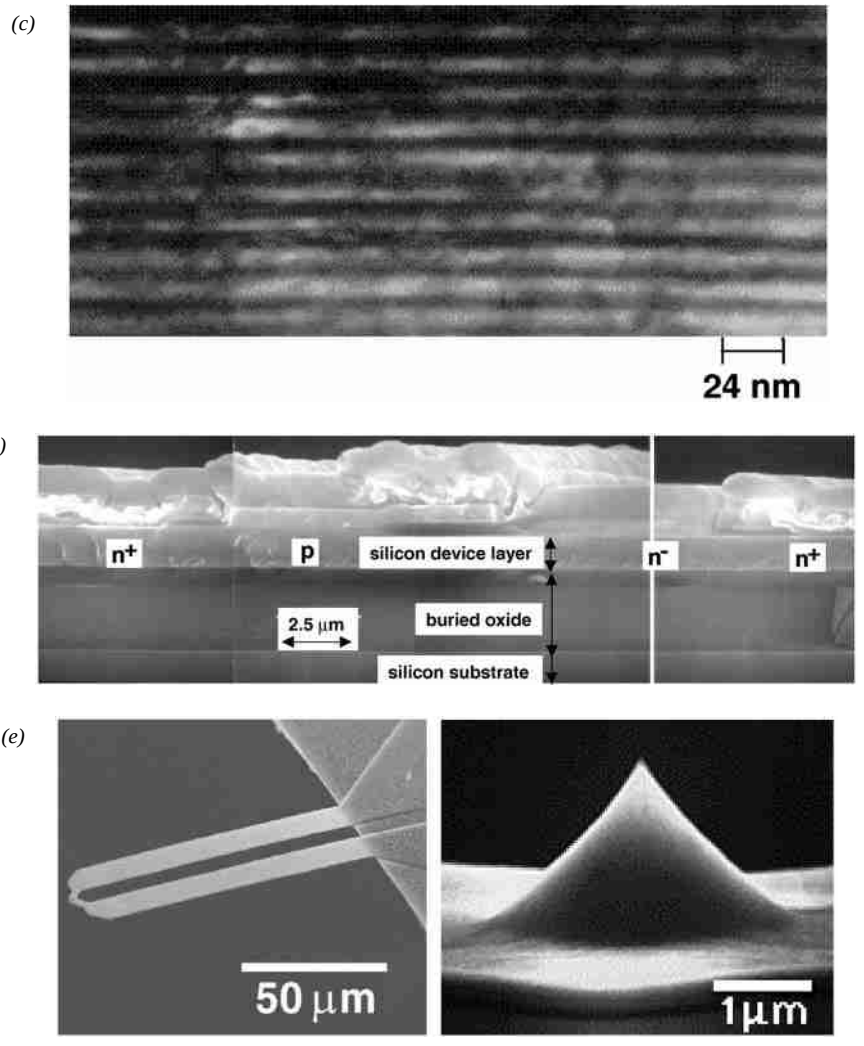

Figure 1 (*Continued*)

polyimide films. Figure 2*b* shows that polyimide films exhibit anisotropic conductivities due to the partial alignment of molecular strands in the film plane (22–25), which is sensitive to the spin-coating parameters. The conduction of atomic vibrational energy is more effective by means of the electronic bonds coupling atoms along a molecule than by the forces acting between neighboring molecules. Figure 2*c* shows that the volumetric heat capacity in silicon dioxide, which influences transient heat conduction, can depend strongly on

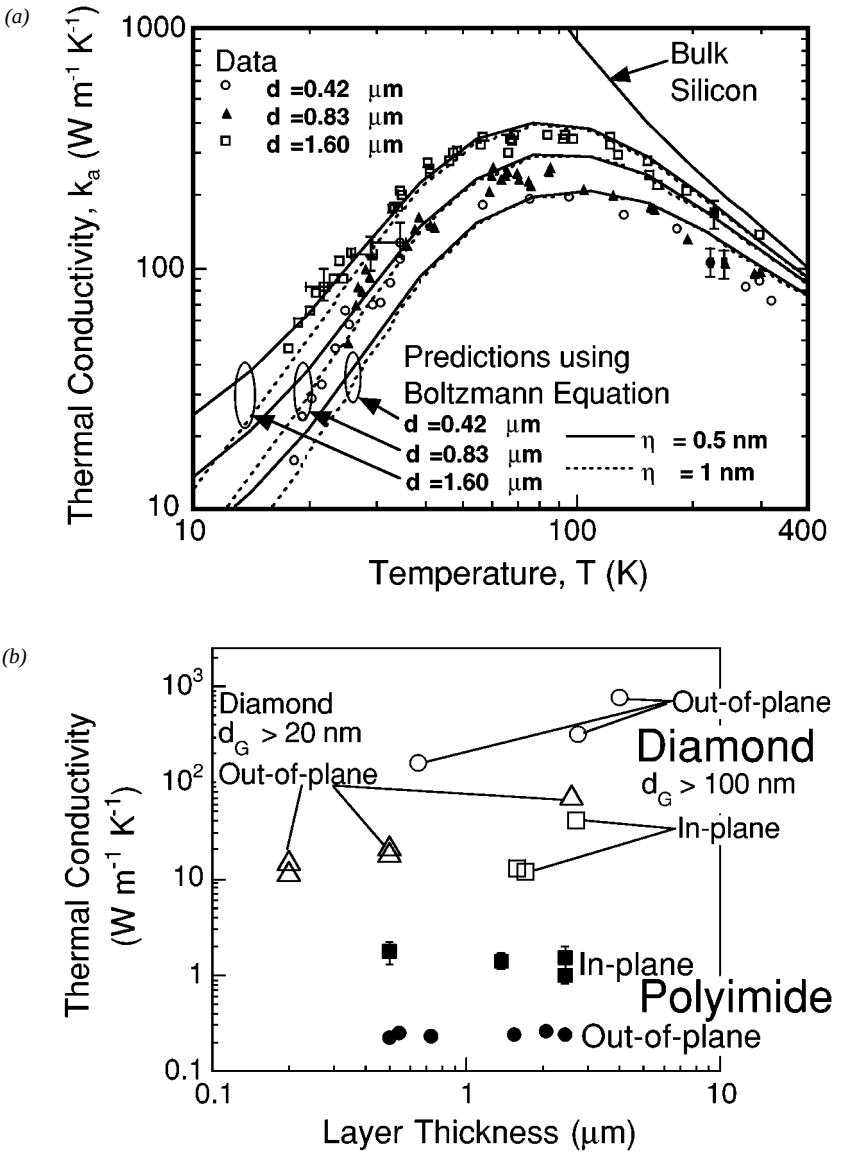
(a)
Thermal Conductivity, k_a (W m^{-1} K^{-1})
1000
100
10
10
100
400
Temperature, T (K)
Data
d =0.42 μm
d =0.83 μm
d =1.60 μm
Bulk
Silicon
Predictions using
Boltzmann Equation
d =0.42 μm
d =0.83 μm
d =1.60 μm
η = 0.5 nm
η = 1 nm
(b)
Thermal Conductivity
(W m^{-1} K^{-1})
10^3
10^2
10
1
0.1
0.1
1
10
Layer Thickness (μm)
Diamond
d_G > 20 nm
Out-of-plane
Out-of-plane
Diamond
d_G > 100 nm
In-plane
In-plane
Polyimide
Out-of-plane

Figure 2

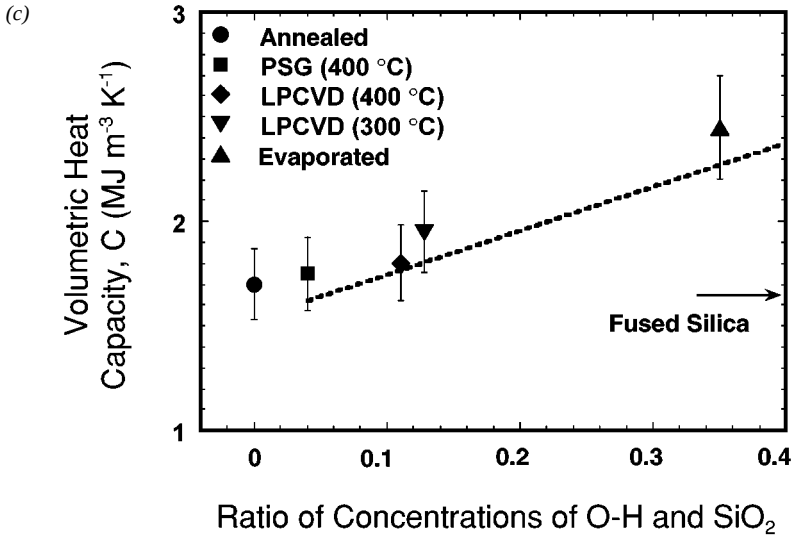

Figure 2 (*Continued*) Data illustrating the thickness and process dependence thin-film thermal properties: (*a*) Influence of phonon-interface scattering on the out-of-plane thermal conductivity of single-crystal silicon-on-insulator films (17, 18). The predictions account for partially specular reflection at the film interfaces with characteristic roughness η. (*b*) Thermal conductivity extremes and contrasting anisotropy in polycristalline diamond (20, 21) and a representative fully amorphous polyimide (24, 25). (*c*) Variation of the volumetric heat capacity with O-H fraction in deposited silicon dioxide films (26).

the concentration of impurities as characterized by Fourier transform infrared spectroscopy (FTIR) and Rutherford backscattering spectrometry (RBS) (26). The O-H bonds originate in part from water, which has much larger volumetric heat capacity than silicon dioxide.

This review describes measurement and modeling research on the thermal conduction properties of electronic films, with emphasis on relatively novel films and on the impact of the structural state of the films. This review discusses only dielectric and semiconducting materials, in which coupled atomic vibrations are responsible for heat conduction. We alert the reader to reviews with related subject material. Cahill et al (27), Swartz & Pohl (28), and Cahill (29) reviewed thermal transport research for dielectric films and their interfaces, including several of relevance for electronic systems. These reviews are most helpful for the study of highly disordered glasses and for their effective use of cryogenic data to investigate the coupling of microstructure and heat transport. Goodson & Flik (30) reviewed film thermal conductivity measurement techniques relevant for electronic systems. Heat conduction studies on deposited

diamond films were reviewed by Graebner (3) and Plamann & Fournier (31), and more recently, with a focus on films thinner than 5 μm, by Touzelbaev & Goodson (4). An overview of heat conduction research on superlattices can be obtained through the articles by Hyldgaard & Mahan (32) and Chen (33, 34). The properties of organic thin films have received surprisingly little attention considering the practical relevance of related optoelectronic devices, although some guidance can be found in monographs on bulk materials (e.g. 35) and a few recent papers (22, 23, 25). Similarly, there has been little research on heat conduction in high-T_c superconducting films, although the reader can gain insight through a review on bulk materials (36) and a few studies relevant for films (37, 38).

METROLOGY

When measuring film thermal conductivities, care must be taken to obtain data that are appropriate for simulating practical devices. Many techniques use a film structure that does not resemble the functional device and, in many cases, requires processing that alters the purity or structural quality of the film. For example, many techniques require free-standing films, which experience a different stress history and are exposed to more contaminants than those within a device. This section reviews techniques that are deemed to be most appropriate for use in conjunction with electronic device design. The techniques described here use either lasers or electrical currents for heating, which offer contrasting advantages. Laser heating avoids contact with the sample film, which helps for small samples and when adhesion is a problem. It is nearly impossible to know consistently the precise magnitude of radiation power absorbed by the film, which renders the absolute magnitude of the temperature response of little use. However, the precise temporal control of intensity, which is made possible through picosecond and nanosecond pulsed lasers and optical modulators, allows thermal properties to be extracted from the temporal response without knowledge of the magnitude. Electrical heating is applied using currents in conducting bridges micromachined on the film. The Joule heating power can be accurately measured and controlled in some cases with resolution below 1 μs.

Electrical heating has been used for films and superlattices with lower thermal conductivities than the underlying substrate. The simplest methods measure the out-of-plane conductivity in layers of thickness near 1 μm using steady-state heating and thermometry in neighboring metal bridges patterned on the sample film (28, 39, 40). More versatility is available through transient electrical-heating methods (19, 24–26, 41, 42), which extend the 3ω method (43) using the geometry shown in Figure 3*a*. A harmonic electrical current in the bridge yields heating and temperature fluctuations at frequencies up to a few tens of kHz, which are detected through the third harmonic of the voltage signal. While

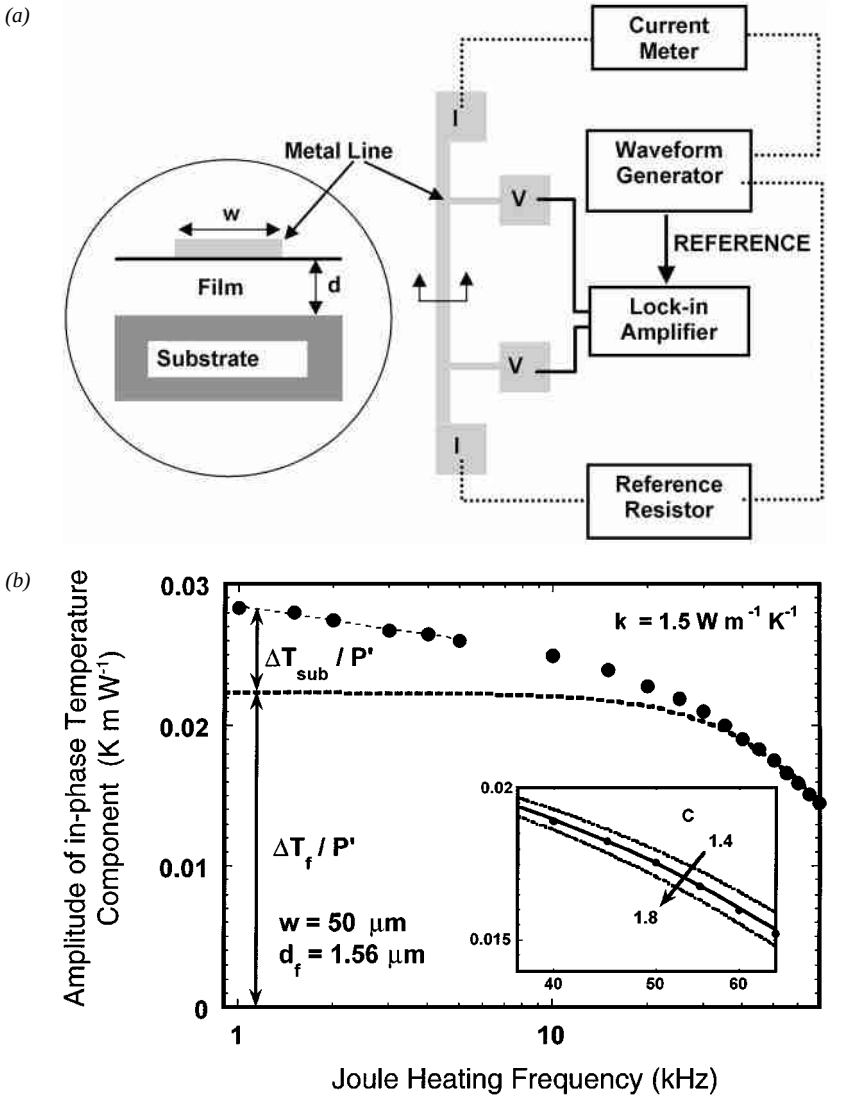

Figure 3 Electrical metrology for thin-film thermal properties: (*a*) Experimental structure and apparatus for 3ω measurements of the out-of-plane thermal conductivity of thin films. Measurements on bridges of varying widths and large heating frequencies are used to extract the in-plane thermal conductivity and the volumetric heat capacity. (*b*) Components of the in-phase temperature amplitude, which is measured using the 3ω technique for silicon-dioxide films and normalized by the power amplitude per unit length P'. The high-frequency data are sufficiently sensitive to the volumetric heat capacity that this property can be extracted. Data for films with varying O-H content are shown in Figure 2*c*.

this approach is used mainly to measure the out-of-plane conductivity, careful choice of layer dimensions and operating frequencies can yield other properties in samples that are sufficiently thick. Measurements using bridges of varying widths w have yielded the in-plane component for polyimide films (24, 25) and for a Si/SiGe superlattice (42), although with a relatively large uncertainty. Data for polyimide films measured using this approach are shown in Figure 2*b*. When the heating frequency is somewhat larger than d^2C/k_n, which is the timescale of heat diffusion normal to the film, it is possible to extract the film volumetric heat capacity as well as k_n (26). The extraction approach for both C and k_n is depicted in Figure 3*b*. The measurement techniques described in this paragraph have been applied to low-thermal-conductivity oxides, organic materials, and superlattices. In contrast, measurements on high-thermal-conductivity silicon films have been made with the aid of a buried, thermally resistive silicon dioxide layer, which is standard in silicon-on-insulator substrates and augments the sensitivity of the metal bridge temperature to lateral transport in the silicon film. This approach was used with steady-state heating for silicon films as thin as 400 nm (17, 18), yielding the data in Figure 2*a*, and with the 3ω approach for silicon films as thin as 80 nm (19).

Pulsed laser heating and laser-reflectance thermometry have been used for noncontact measurements of the out-of-plane thermal conductivity in thin films, as depicted in Figure 4*a*. The instrumentation and analysis differ substantially depending on the duration of the heating pulse. Measurements with picosecond-scale heating, e.g. from a Ti:Sapphire laser, have been applied to GaAs/A1As superlattices (44), diamond-like carbon (45), and metal films (46). These measurements use pump-probe laser diagnostics for the temperature, and analysis must decouple the responses from the near-surface temperature rise and acoustic propagation. The analysis must also consider the nondiffusive nature of heat transport in the sample films and the disequilibrium between electrons, which can absorb most of the radiation, and the lattice. The extraction is simplified somewhat for measurements using nanosecond-scale heating, e.g. from a ND:YAG laser, during which acoustic waves are fully attenuated. Nanosecond heating and continuous time-domain laser-reflectance thermometry yielded the out-of-plane conductivities of silicon-dioxide (47) and polycrystalline diamond (20, 21, 48) films of thickness down to a few hundred nanometers. The drawbacks of this approach include the time-domain noise from the detector and associated electronics. Depending on the relative thicknesses of the absorbing layer and the underlying film, the measurements can be insensitive to the volumetric heat capacity of the sample layer. One benefit of laser heating is that the brief pulse duration helps to decouple the properties of the substrate from the film. This facilitates measurements on films with much higher thermal conductivities than the underlying substrate, such as the

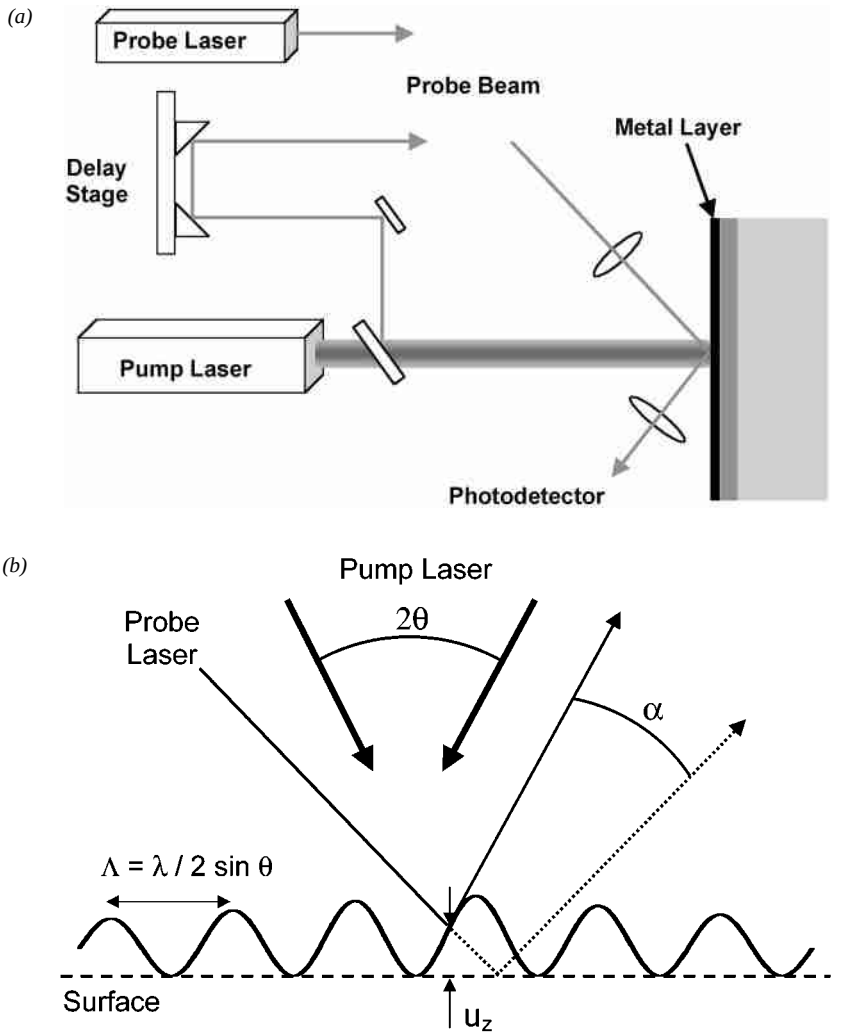

Figure 4 Optical metrology for determining the thermal properties of thin films: (*a*) Flash heating for the study of out-of-plane transport. These methods use either a steady probe laser or pump-probe diagnostics. (*b*) Distribution of radiation intensity and vertical thermomechanical displacement, u_z, for lateral transport measurements using transient gratings. The interrogation depth into the sample increases with the spatial period of the energy absorption on the surface, which is governed by the wavelength λ_R and the separation angle 2θ of the incident radiation beams.

diamond film with $k_n = 600$ W m^{-1} K^{-1} investigated by Verhoeven et al (21) on a silicon substrate.

The lateral thermal conductivity of films on substrates has been measured using the transient thermal grating technique (21, 49, 50), which is depicted in Figure 4*b*. Pulsed laser radiation interferes on the sample surface, yielding a harmonic spatial variation of energy absorption. This yields spatially varying temperature and thermomechanical displacement fields, whose temporal decay is detected by the deflection of an incident probe beam. The temporal decay is governed mainly by the lateral thermal conductivity and the volumetric heat capacity of the film and substrate within a depth near the spatial period of energy deposition, which can be varied by altering the angle θ. This technique resembles the approach used for free-standing polyimide films of Rogers et al (23), although the property extraction theory for films on substrates is substantially more complicated.

MODELING

Figure 5 provides an overview of the hierarchy of modeling approaches that have been applied to single- and polycrystalline dielectric and semiconducting films. The minimum lengthscales considered by these simulations are distinguished by comparison with both the phonon wavelength λ and the phonon mean free path Λ. The complexity of phonon dispersion relationships, anharmonic interactions, and scattering on imperfections and interfaces makes the existing theories only partially satisfactory in explaining available data. The complexity yields so many degrees of freedom in a given theory that agreement with data can sometimes be misleading. This section briefly describes the major modeling approaches and provides a framework for more detailed discussion in subsequent sections relating to specific materials.

Atomistic calculations have been used to study the lattice dynamics and the thermal properties of dielectric materials. In the case of crystalline materials, ab initio calculations yield phonon spectra, from which the volumetric heat capacity, the Grüneisen parameter, and the thermal expansion coefficient can be calculated (51). Atomistic simulations are also useful for studying the vibrational characteristics of amorphous dielectric materials (52). In contrast, atomistic calculations of thermal conduction (53) have had limited impact, due in part to the lack of accurate interatomic potentials for technically important materials. Currently available interatomic potentials do not accurately describe phonon spectra and anharmonic interactions in silicon (54).

The atomistic approach is having some impact on our understanding of phonon-interface interactions, which strongly influence thermal conduction. Molecular dynamics simulations examined the role of inelastic phonon scattering

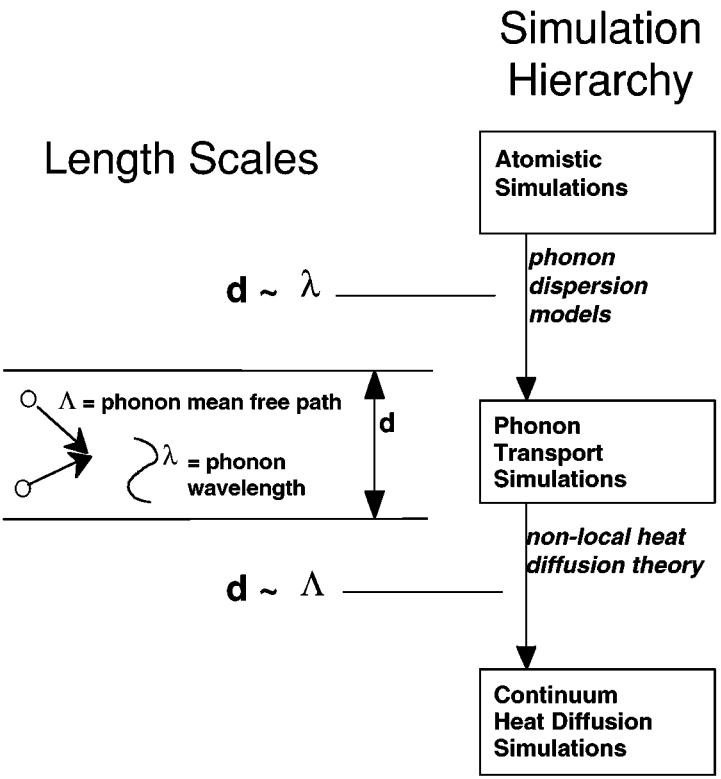

Figure 5 Modeling hierarchy for thin dielectric films.

on heat transport across diamond-metal interfaces (55). Atomistic calculations were used to study phonon dispersion and modified anharmonic coupling in superlattices (14–16), which are important when the superlattice period is comparable to the wavelengths of a significant fraction of thermal phonons. Recent calculations can be found for Si/Ge (56) and GaAs/A1As (32) superlattices. Related work is approaching the dispersion relationship problem from the perspective of wave theory (57, 58) by predicting the impact of phonon interference and confinement. These calculations yield folded phonon zones and can predict large reductions in transport. When strictly defined, the lengthscale for the onset of wave interference effects is the coherence length, which is comparable to the wavelength and describes the distance over which phonons have comparable phase (59). Subsequent sections in this review show that, at least according to the experimental evidence for contemporary electronic films and superlattices, phonon interference and modified dispersion

phenomena are less important than phonon scattering on imperfections and thin-film interfaces.

Most device simulations use heat-diffusion theory, which is based on the Fourier heat-conduction law, together with measured or predicted effective thermal conductivity values for constituent films. The conductivity values are predicted or interpreted using solutions to the phonon transport equation, either in a classical form for bulk materials (60, 61) or in more complicated expressions that account more rigorously for phonon-interface scattering in thin films and superlattices (62–64). Interface scattering is important when a significant fraction of thermal phonons have free paths comparable with or somewhat larger than the film thickness. Phonon transport simulations generally assume the crystal to be isotropic and collapse the phonon-interface interaction physics into a parameter describing the degree of specular reflection by the interface.

For crystalline dielectric materials, the simplest form of the phonon transport theory relies on an analogy with gases. The kinetic theory yields

$$k = \frac{1}{3} C\, v\, \Lambda, \qquad 1.$$

where the volumetric heat capacity C and the average phonon speed v, which is approximately given by the speed of sound, can be determined from experimental data. The phonon mean free path Λ is the average distance traveled by phonons between anharmonic interactions with other phonons or scattering events with imperfections, electrons, and impurities. Several of these scattering mechanisms are depicted in Figure 6. Equation 1 neglects the strong dependence of the phonon speed and mean free path on frequency and branch. More

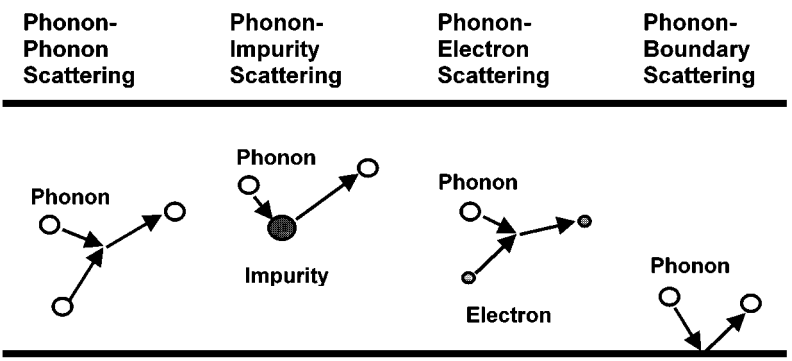

Figure 6 Phonon scattering mechanisms in thin films.

detailed modeling uses (60, 61)

$$k = \sum_i \frac{1}{3} \int_0^{\theta_{D,j}/T} C_i(x) v_i^2(x) \tau_i(x) dx + k_n, \qquad 2.$$

where $\tau = \Lambda/v$ is the phonon relaxation time, $x = \hbar\omega/k_B T$ is the dimensionless phonon frequency, k_B is the Boltzmann constant, and $\hbar$ is Planck's constant divided by 2π. The integral weights the frequency-dependent phonon relaxation time by the phonon-specific heat function, which is usually based on Debye theory. More detailed calculations can account for phonon dispersion through more detailed models for the frequency dependences of $C_i(x)$ and v. The summation is over the two transverse and the single longitudinal phonon polarizations, for which the frequency-dependent specific heat function and Debye temperatures θ_D can be calculated from the properties of shear and longitudinal acoustic waves, respectively. The conductivity k_n is a correction term that Callaway (60) introduced to account for the nonresistive nature of phonon normal processes. Equation 2 neglects the directional dependence of the acoustic properties in a solid. The phonon scattering rate $1/\tau$ is calculated using Matthiessen's rule

$$\tau_i^{-1} = \sum_j \tau_{i,j}^{-1}. \qquad 3.$$

The summation accounts for the scattering mechanisms shown in Figure 6, i.e. phonon-phonon scattering, phonon scattering on imperfections or impurities, and phonon-electron scattering. Equation 3 can also be augmented to account for scattering on thin film and grain boundaries using $\tau \sim d/v$, where d is the characteristic film or grain size. Subsequent sections of this review show that more detailed models are available for handling scattering on film and superlattice interfaces and grain boundaries. For superconducting materials, Equation 3 can be augmented to account for phonon scattering with the fraction of the electron gas remaining in the normal state at a given temperature (36, 65, 66).

For highly disordered materials, a large fraction of the phonons carrying heat near room temperature are not well defined because of their short relaxation times (67). For this reason, the phonon model is not very well suited for linking diffusion theory with atomistic calculations as depicted in Figure 5. At temperatures above the thermal-conductivity plateau region, several heat conduction mechanisms have been proposed to be active, in addition to that associated with the propagating modes described by Equation 2. Some studies (68) considered the hopping of localized vibrational excitations, which occurs via anharmonic interactions with phonons. Other research (69, 70) focused on heat transport by diffusive as opposed to localized vibrational excitations. A generalized Einstein model (71) considered the random walk of thermal energy between localized

oscillators, which may be considered equivalent to diffusive transport. This model has been particularly useful for predicting the minimum thermal conductivity of highly disordered crystals.

SINGLE-CRYSTAL FILMS AND SUPERLATTICES

This section discusses measurement and modeling examples for heat conduction in single-crystal electronic films and superlattices. In-plane conduction was most extensively investigated for silicon films of thickness between 80 nm and about 1 μm in SOI wafers. This section also discusses the rapidly growing number of thermal conduction models and data for both in-plane and out-of-plane transport of GaAs/AlGaAs and Si/Ge and related alloy superlattices. Finally, this section concludes with a few words about high-T_c superconducting films, in which both phonons and electrons can contribute significantly to heat conduction.

SOI technology offers complete dielectric isolation and promises enhanced performance for semiconductor devices in both high-power and low-power circuits (72). SOI wafers are made using bonding and etch-back technology, implantation of oxygen in silicon (73), and more exploratory lateral growth or implantation methods (74, 75). These wafers provide an opportunity to investigate phonon-interface scattering in films that, at least in comparison with other films and superlattices discussed in this review, contain low concentrations of lattice imperfections. Phonon-interface scattering has a dramatic impact on heat conduction in SOI thin films below room temperature. Figure 2*a* shows the predictions and data of Asheghi et al (17, 18), who measured the thermal conductivities of SOI layers at temperatures between 20 and 300 K. The predictions are based on the model of Holland (61) for conduction in silicon, which is similar to Equations 2 and 3, and account for phonon-interface scattering. The relaxation time for the film is reduced by a solution to the phonon transport equation (76)

$$\frac{\tau_{film}}{\tau} = 1 - \frac{3(1-p)}{2\delta}\int_1^\infty \left(\frac{1}{\xi^3} - \frac{1}{\xi^5}\right)\frac{1-\exp(-\delta\xi)}{1-p\exp(-\delta\xi)}d\xi, \qquad 4.$$

where $\delta = d/\Lambda = d/v\tau$, d is the layer thickness, and p is the fraction of phonons specularly reflected by the film boundaries. Equation 4, with $p = 1$, yields the ideal limit of completely specular reflection for which no reduction in the conductivity is expected. The use of $p = 0$ yields completely diffuse scattering, which minimizes the conductivity for a given film thickness. Although there is reasonable agreement between the predictions and data for the thickest layer, with $d = 1.5$ μm, the disagreement is substantial for the thinner layers. One possible explanation for the discrepancies is larger concentrations

of imperfections in the film than in the bulk material. However, since imperfections could be expected to collect near the film interfaces, their impact and the degree of overprediction would be expected to increase with decreasing film thickness. This trend is not found in Figure 2*a*, which suggests that the excellent agreement for the thickest film may be fortuitous. However, the general trend of the conductivity with temperature is predicted with a reasonable degree of accuracy, which indicates that Equations 2 and 4 describe the dominant physics of the interface scattering problem in a single film.

Transport modeling is most poorly understood at elevated temperatures, where the complexity and anisotropy of the phonon dispersion relationship more strongly influence transport. The complications become substantial near about 100 K for GaAs, Ge, and AlAs, and near about 200 K for Si due to its higher Debye temperature. Figure 7*a* plots room-temperature in-plane thermal-conductivity data for silicon layers in SOI substrates as thin as 80 nm (19). The thermal conductivity is smaller than the bulk value by as much as 50% and decreases with decreasing film thickness. Figure 7*a* also includes three simple model calculations (19) that assume totally diffuse scattering, $p = 0$. A graybody approximation, which combines Equations 1 and 4, overpredicts the conductivity because it neglects the spectral dependence of phonon scattering (77). The second model assumes that longitudinal phonons dominate conduction and yields better agreement. This approach is motivated by the dispersive nature of high-frequency transverse acoustic phonons in silicon, which reduces their group velocities. Recent studies suggest that high-frequency transverse acoustic phonons contribute little to conduction due to their strong scattering on point defects (78). The calculation in Figure 7*a* assumes that isotopic impurities and anharmonic interactions dominate internal scattering. The phonon-phonon scattering rate varies with frequency according to $\tau^{-1} \sim \omega^m$. The exponent $m = 1.7$ is extracted from conductivity data for samples of Ge, which has phonon spectra very similar to those of silicon, with varying concentrations of electrically neutral impurities. The data are at least consistent with this model calculation, which supports the hypothesis that high-frequency longitudinal phonons with short mean free paths contribute strongly to heat transport above room temperature in silicon.

The thin-film boundary conditions for phonon transport analysis warrant careful consideration. Equation 4 neglects participation by the bounding materials, which are amorphous silicon dioxide for the case of the SOI film studies described here. Using the theory of radiation reflection with interfaces, an expression for the specularity factor can be derived that decreases exponentially with the square of the ratio of the characteristic interface roughness, η, to the phonon wavelength (12). Figure 2*a* shows that the predictions do not differ substantially even at low temperatures for two typical interface roughnesses,

(a)

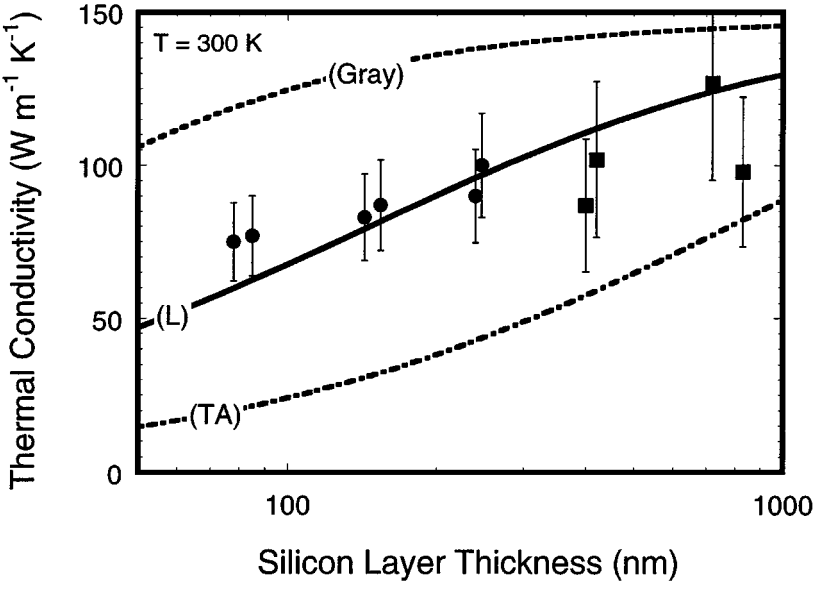
T = 300 K
(Gray)
(L)
(TA)
Thermal Conductivity (W m-1 K-1)
150
100
50
0
100
1000
Silicon Layer Thickness (nm)

(b)

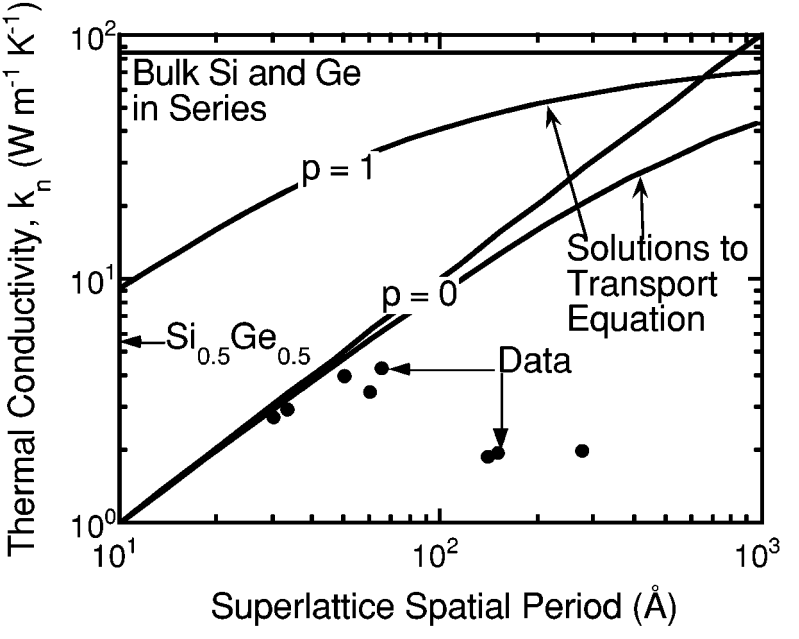
Bulk Si and Ge
in Series
p = 1
p = 0
Solutions to
Transport
Equation
Si0.5Ge0.5
Data
Thermal Conductivity, kn (W m-1 K-1)
10^2
10^1
10^0
10^1
10^2
10^3
Superlattice Spatial Period (Å)

Figure 7

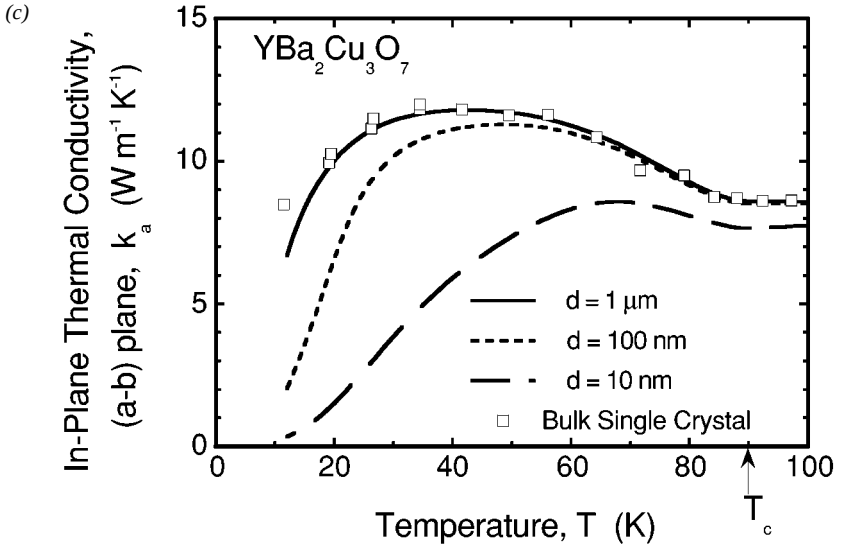

Figure 7 (*Continued*) Room-temperature thermal conductivities of single-crystal films and superlattices: (*a*) Predictions and data for conduction along SOI device layers (19). (*b*) Predictions of Chen (*heavy lines*) (33) for conduction normal to Si/Ge superlattices, compared with data of Lee et al (*filled circles*) (80). (*c*) Predictions of the in-plane thermal conductivity reduction due to electron and phonon scattering on interfaces in $YBa_2Cu_3O_7$ films (38).

which suggests that phonon scattering can be modeled as completely diffuse. This approach is an idealization, however, because the SOI layer exchanges phonons with the bounding silicon-dioxide film. However, it can be argued that because phonons are scattered so strongly in silicon dioxide, this material acts as a diffuse black phonon emitter and absorber with $p = 0$. When the mean free paths in neighboring films are comparable, which is the case in many superlattices, this approximation and Equation 4 are no longer valid.

Chen (79) has derived expressions accounting for lateral transport along crystalline superlattices, which are based on the Boltzmann transport equation and consider the degree of specularity in phonon exchange at the periodic interfaces. For completely specular reflection at the interfaces of materials with similar elastic constants, the thermal conductivity can be comparable to that of parallel films of the two materials without interface scattering, which is simply an average of the two bulk conductivities. This is analogous to the predictions of Equation 4 for a single film with $p = 1$. Completely specular reflection is unlikely at room temperature given the relatively short wavelengths of phonons, even for the best superlattices, such that predictions for partially or

fully diffuse reflection are expected to be more appropriate. This is consistent with recent measurements on a $Si/Si_{0.71}Ge_{0.29}$ (5 nm/1 nm) superlattice, whose lateral thermal conductivity was 60% smaller than the appropriate weighted average of bulk properties (42). However, it is not known if the reduction is caused by interface scattering or by imperfections within the layers. Another complicating phenomenon at superlattice interfaces is the possibility of the confinement in one layer of phonons, whose frequencies lie beyond the frequency maximum of the acoustic branches in the bounding solid.

Although heat conduction normal to single-crystal films is being investigated most extensively for those in superlattices, there remains a very large gap between phonon transport predictions and data. This problem owes much to large concentrations of imperfections that occur during the growth process due to the mismatch of lattice constants in the constitutent films. Superlattices also highlight any problems with the assumed phonon-interface scattering behavior. The key distinctions are between specular and diffuse reflection and transmission at an interface, which has already been discussed in this section, and between elastic and inelastic scattering. Elastic scattering assumes that phonons striking an interface must depart with the same frequency, such that there is no energy transfer among different modes. Fully elastic scattering underpredicts the rate of heat conduction because it neglects the anharmonic interfacial coupling among different modes, which can be simulated using atomistic calculations (55). Fully inelastic scattering overpredicts the rate of heat conduction because it neglects the confinement of phonons in layers with higher Debye temperature. Chen (33) has illustrated the impact of these boundary conditions by solving the Boltzmann transport equation. The simplest result neglects scattering within the layers and assumes fully diffuse, fully inelastic scattering, yielding

$$k_n = \left(\frac{C_1 v_1 C_2 v_2}{C_1 v_1 + C_2 v_2} \right) \left(\frac{d_1 + d_2}{2} \right), \qquad 5.$$

where the subscripts 1 and 2 denote parameters of the two repeating films in the superlattice. Equation 5 is approximate because it neglects the frequency dependence of scattering and does not explicitly distinguish between the transport characteristics of optical and acoustic phonons. Equation 5 and more rigorous calculations are compared with the data of Lee et al (80) for pure Si/Ge superlattices in Figure 7*b* (81). The model is consistent with the data for the smaller superlattice period, although the results for thicker films disagree substantially. This may result from larger concentrations of imperfections within the layer than are not present in the bulk materials, which may occur when the superlattice period is too large to allow the material to sustain lattice-mismatch strain. Figure 7*b* supports the conclusion that interface scattering is predominantly diffuse. The data also suggest that the highly strained superlattices based

on pure films contain a much higher concentration of imperfections than superlattices containing alloys (42). More modeling and measurements must accompany material fabrication work to resolve the role of the lattice imperfections in reducing the thermal conductivity.

Epitaxially grown high-T_c superconducting films, such as $YBa_2Cu_3O_7$, $EuBa_2Cu_3O_7$, and $BiSr_2Ca_1Cu_2O_8$, exhibit highly anisotropic thermal conduction properties due to their orthorhombic unit cell and the large density of oriented imperfections. These films are promising for low-loss interconnects and Josephson junctions in hybrid superconductor/semiconductor circuits, as well as for thermal radiation detectors (82). Although there are few if any data available for the thermal conductivity along thin superconducting films, there have been several measurements of the thermal interface resistance with underlying substrate materials (83). The bulk properties and anisotropy have been well documented (84–89), and models have been developed for the conductivity reduction in films with the *c* axis oriented normal to the substrate (37, 38). These calculations needed to consider the simultaneous contribution of electrons and phonons, because both carriers are significant at temperatures above a few tens of Kelvin. The electron contribution in $YBa_2Cu_3O_7$ was found to be approximately 50% of the total conductivity at the transition temperature, 90 K. The reductions in electron and phonon transport were estimated independently using Equation 1 and an approximate model accounting for interface scattering (38). Figure 7*c* plots the temperature dependence of the thermal conductivity for films of varying thickness. This calculation neglected the anisotropy of the acoustic properties of the sample, which could be expected to diminish the size effect, and the spectral dependence of the phonon mean free path, which underestimates the size effect. However, this model illustrates the anticipated physics. The reduction is substantial for films thinner than about 100 nm and is dominated by the impact of interfaces on the phonon contribution. The electron thermal conductivity and associated thin-film size effect is strongly reduced at low temperatures due to the increasing concentration of Cooper pairs, which do not contribute to heat conduction.

POLYCRYSTALLINE FILMS

In polycrystalline films, internal scattering can overwhelm the film-boundary scattering discussed in the previous section. Increased rates of internal scattering result from the grain boundaries and, in some cases, from lattice imperfections and impurities that occur with high densities near grain boundaries. The polycrystalline thin-film material whose thermal properties have received the greatest attention is chemical-vapor-deposited diamond. While most research has focused on diamond layers thicker than about 30 μm (3, 31), there has also

been progress on characterizing both the in-plane and out-of-plane thermal conductivities of films thinner than 5 μm (4). This section uses the data for these relatively thin films as a representative study of the impact of enhanced phonon scattering in polycrystalline dielectric films.

The simplest approach to modeling phonon scattering on grain boundaries is to augment the scattering rate in Equation 3 by

$$\tau_G^{-1} = B\frac{v}{d_G}, \qquad 6.$$

where B is a dimensionless parameter that increases with the phonon reflection coefficient at grain boundaries and varies with the grain shape. The mean free path calculated using Equation 6 is $\Lambda = d_G/B$, where d_G is the characteristics grain dimension. Figure 8*a* shows that d_G, which is estimated from electron micrographs such as Figure 1*a*, varies strongly with the separation from the substrate. For phonons with wavelengths that are long compared with the size of strained region around the boundary, the reflection coefficient is independent of the phonon wavelength and comparable with $(\Delta v/v)^2$, where Δv is the difference in acoustic velocities in the crystal directions for the incident and refracted paths (12). The minimum grain size d_{G0}, which varies from a few tens of nanometers to about a micrometer, is approximately given by the inverse square root of the nucleation density. This density is controlled by the substrate material and the nucleation method, which ranges from the use of a bias voltage between the microwave source and the substrate (90) to the use of acoustic agitation with a diamond-laden slurry (1). Depending on the details of the nucleation process, it can be necessary to account for the thickness of disordered material near the substrate (91).

However, Equation 6 is overly simplistic for relatively defective polycrystalline films. For example, Equation 6 is questionable for diamond films because there is no corresponding signature in the measured temperature dependence of the low-temperature thermal conductivity (92). At temperatures above a few degrees Kelvin, the rate of phonon scattering on distinct grain boundaries, which is independent of the phonon frequency, was found to be much smaller than the rate of scattering on other types of defects, e.g. impurities, which depends strongly on the phonon frequency. This is consistent with electron backscattering and transmission micrographs for single-diamond grains (93, 94), which show high concentrations of twin boundaries, dislocations, stacking faults, point defects, and regions of non-diamond phase near the grain boundaries. The densities of these imperfections are closely coupled to the size and orientation of grain boundaries in the films.

If these imperfections occur predominantly near grain boundaries, the phonon scattering rate can still be coupled to the grain size d_G. This concept was given

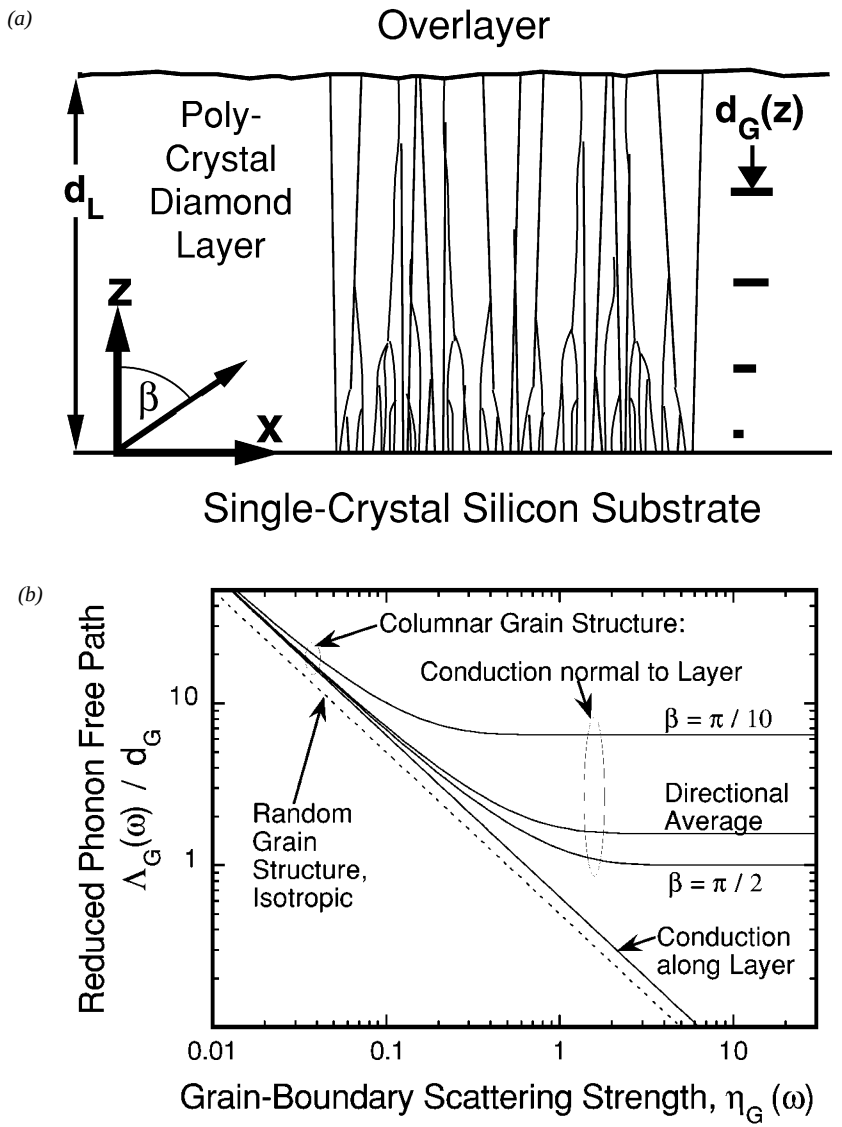

Figure 8 Grain structure and phonon scattering in polycrystalline CVD diamond layers: (*a*) Schematic showing the columnar grain structure found in many diamond films deposited on silicon. This diagram defines the angle β for phonon trajectories with respect to the normal coordinate in the film. (*b*) Predictions for the variation of the phonon mean free path with the grain size (64).

a mathematical framework by Goodson (64), who defined the dimensionless grain-boundary scattering strength,

$$\eta_G = \sum_j \sigma_j \, n_j . \qquad 7.$$

The frequency-dependent cross section and number density per unit grain-boundary area of imperfection j are denoted as σ_j and n_j, respectively. The scattering rate for randomly oriented grains is given by Equation 6 with $B = 2\eta_G$, which assumes that defects associated with a given grain boundary are distributed uniformly within grains. This simple form overpredicts the scattering rate for transport normal to films with columnar grains, for which imperfections near grain boundaries can have a relatively small influence on conduction. An average of phonon free paths over all directions in a columnar grain is well approximated by

$$\tau_G^{-1} = \frac{2v}{\pi d_G} \left[1 - \exp\left(-\frac{\pi^2}{4} \eta_G \right) \right], \qquad 8.$$

which yields a scattering rate with an upper bound dictated by the grain size. The models for the variation of the phonon mean free path with grain size are plotted in Figure 8*b*.

Figure 9 compares the data for the vertical thermal resistance of thin layers with calculations using Equations 2, 3, 7, and 8. The scattering strength is governed by point and extended defects with cross sections taken from research on thicker diamond films (3). The calculations are most successful for films deposited at high temperatures, because a single grain-boundary scattering strength yields agreement with a broad variety of grain sizes without any additional adjustable parameters. Scattering is neglected within the grains. However, agreement for films deposited at lower temperatures requires the use of an internal scattering term, which is independent of the grain size. This suggests that lower deposition temperatures diminish the purity and microstructural quality deep within grains, which is consistent with larger concentrations of non-diamond carbon observed through Raman spectroscopy (95, 96). The impact of processing conditions on lateral transport in thin diamond layers can be even more extreme, as has been reviewed previously (4). To our knowledge, there is only one study reporting both the in-plane and out-of-plane thermal conductivities of a given set of diamond films. Verhoeven et al (21) observed a particularly large degree of anisotropy for films with predominantly heteroepitaxial grains, with the in-plane conductivity smaller by about one order of magnitude than the out-of-plane conductivity. Representative data from that study are included in Figure 2*b*.

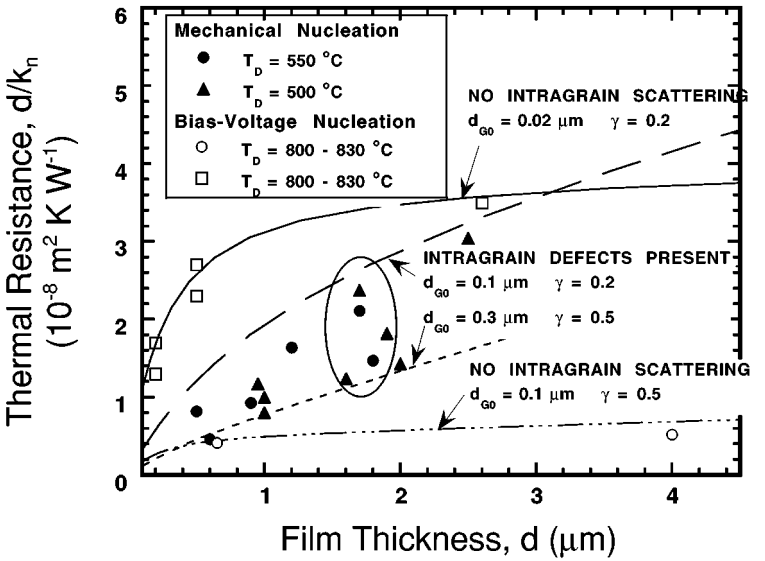

Figure 9 Dependence of the out-of-plane thermal resistance of polycrystalline CVD diamond films on the nucleation method and the film thickness (4). The grain size is assumed to vary linearly with the vertical coordinate, $d_G = d_{G0} + \gamma z$. The minimum grain size d_{G0} and spatial growth derivative γ are estimated from electron micrographs for the films. The predictions are based on the grain-boundary scattering strength model (64, 91).

HIGHLY DISORDERED FILMS

Process compatibility issues motivate the deposition of many dielectric films at low temperatures, which can lead to microstructures and even stoichiometry very different from those found in bulk samples. The influence of these differences on thermal transport properties is important not only for the process optimization but also for study of the minimum thermal conductivity (71). A discussion of the roles of structure and stoichiometry can be most clearly presented for deposited silicon-dioxide films, for which the most thermal conductivity and structural characterization data exist. This section discusses representative data for silicon-dioxide films and then briefly describes other phenomena, such as molecular strand orientation, which influence transport in organic films.

A number of authors have investigated the out-of-plane thermal conductivities of silicon-dioxide films prepared using different methods (26, 39, 41, 97–99). These studies reported reductions in the conductivity by as much as 50% from the value in bulk fused silica. Figure 10*a* summarizes representative data on silicon-dioxide films at room temperature, for which density data are

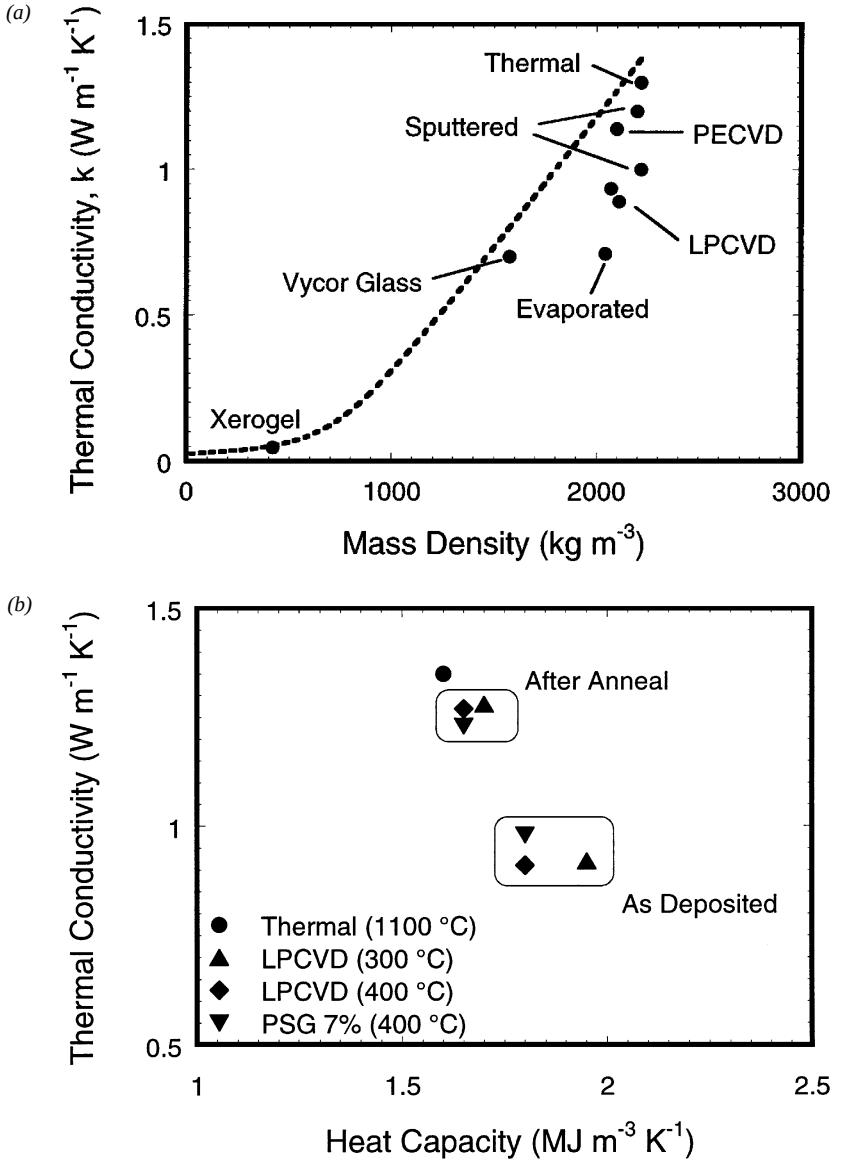

Figure 10 Process-dependent thermal properties of silicon dioxide films, which serve as representative fully amorphous films for the present review: (*a*) Density dependence of out-of-plane film thermal conductivity data (41, 97, 98) compared with predictions from the effective medium theory and data for porous silica glass (100) and a xerogel (101). (*b*) Variation of the volumetric heat capacity and the thermal conductivity with fabrication technique (26).

also available. Shown as a *dotted line* (Figure 10*a*) is the prediction of the effective medium theory, which models the density deficit and thermal conductivity reduction using spherical microvoids uniformly distributed within a fully dense matrix. In contrast to the case for Vycor (100), which is bulk porous glass, the reduction in the thermal conductivities of the silicon-dioxide films cannot be accounted for by the consideration of porosity alone.

Several explanations have been proposed for the observed variations in the out-of-plane thermal conductivities of silicon-dioxide films and the departure from the effective medium theory. One explanation is that the density deficit occurs at an atomic scale (102) and is not well modeled by a theory for macroscopic pores.

Recent measurements indicated that, when corrected for impurities and the density deficit, the volumetric heat capacity of LPCVD silicon-dioxide films does not depend strongly on processing history (26). Figure 10*b* shows the volumetric heat capacities of the LPCVD and e-beam evaporated films, which are actually larger than that of bulk-fused silica owing to the presence of impurities, such as water and silanol. While the excess volumetric heat capacity correlates well with the concentration of O-H bonds in the films, as shown in Figure 2*c*, the effect of these impurities on the thermal conductivity was found to be insignificant. The same study also found that anisotropy in the LPCVD films is negligible, which essentially rules out highly oriented microvoids as a possible cause of the thermal conductivity reduction.

Interesting observations have been made about the impact of high-temperature annealing on the local atomic structure and thermal conductivity of CVD silicon-dioxide films. Following a high-temperature anneal, the root-mean-square deviations of bond lengths, which can serve as a measure of the degree of disorder, diminishes considerably and approaches those of thermally grown silicon-dioxide films. This structural change was shown to be accompanied by a corresponding increase in the thermal conductivity. The connection between the structural disorder and thermal conductivity was also established by previous theoretical studies, which numerically calculated diffusivities of lattice vibrations in model structures with differing amounts of disorder (68, 69).

The thermal properties of organic films are expected to be highly sensitive to their chemical composition and structural configuration. These materials can be semi-crystalline, such that the conductivity depends on the degree of orientation of crystalline regions and of the molecular strands in the amorphous regions. The nature of disorder in organic films renders most of the modeling concepts discussed in this review inappropriate at room temperature. The relevant lengthscales for observing size effects, such as the anisotropy shown for polyimide films in Figure 2*b*, are not known. Although the molecular weight and the molecular radius of gyration might be assumed to play a role, there has been no systematic study of thermal transport in organic films as a function

of these parameters. Past studies of the conductivity (22, 23, 25) focused primarily on demonstrating anisotropy and were not accompanied by detailed spectroscopy. However, some progress can be made using the extensive literature on heat conduction in bulk organic materials, which has been reviewed by Ward (35) and Kurabayashi & Goodson (103).

The series model (104, 105) can be used to interpret thermal conductivity anisotropy data for organic films. The molecular strands are modeled locally within the material as elongated segments with anisotropic intrinsic conductivities. The longitudinal conductivity $k_{a,f}$ describes the transport of atomic vibrational energy along a strand, and the lower out-of-plane conductivity $k_{n,f}$ is used to model the weaker coupling between neighboring strands. While these two conductivities would be extremely difficult to observe experimentally for a single strand, they can be considered equal to the strand-parallel and strand-normal conductivities in a polymer consisting of perfectly oriented molecules. The anisotropy in the material is then given by

$$\frac{1}{k_n} = \frac{1}{2}\left[\left(\frac{1}{k_{a,f}} + \frac{1}{k_{n,f}}\right) - \left(\frac{1}{k_{a,f}} - \frac{1}{k_{n,f}}\right)\langle\cos^2\varphi\rangle\right]; \quad 9.$$

$$\frac{1}{k_a} = \left(\frac{1}{k_{a,f}} - \frac{1}{k_{n,f}}\right)\langle\cos^2\varphi\rangle + \frac{1}{k_{n,f}}. \quad 10.$$

The angle φ is between the film normal and a given strand direction. The operator $\langle\,\rangle$ yields the average cosine considering all strands, is calculated from an assumed orientation distribution function for the polymer strands, and reduces to one third for perfectly random orientation. Figure 11 shows that by assuming a Gaussian distribution function together with Equations 9 and 10, the conductivity anisotropy can be predicted from the standard deviation in the angle of molecular segments with respect to the in-plane direction (105). These results will be much more helpful when more basic modeling principles can be substituted for the intrinsic strand conductivities. Modeling is even more complicated for semi-crystalline polymers, for which the properties and volume fractions of the crystalline and amorphous regions add additional degrees of freedom (106).

CONCLUDING REMARKS

Research on heat conduction in novel films benefits from the characterization tools available from the materials science community. This is of particular importance for mono- or polycrystalline films whose thermal transport properties depend sensitively on structural quality and interface topography. Examples of this connection are presented in this review. The size and orientation of grains

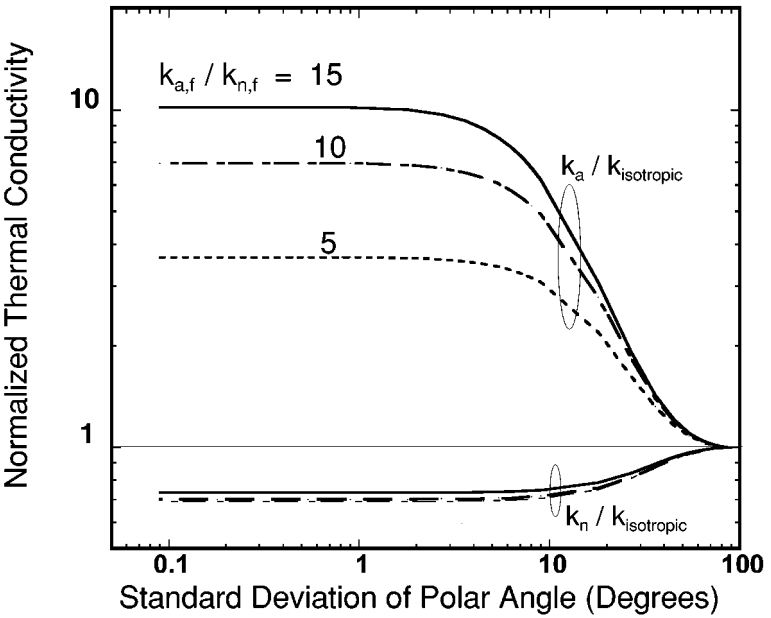

Figure 11 Predictions for the thermal conductivity anisotropy in fully amorphous polymer films (105).

extracted from electron backscattering measurements are shown to strongly influence the thermal conductivity of CVD diamond layers. Superlattice interfaces, which strongly influence heat transport, can be examined through transmission electron microscopy (TEM) or Brillouin scattering measurements. Structural and compositional characterization also can be helpful in the study of certain highly disordered films. Figure 2*c* shows that the volumetric heat capacity of silicon-dioxide films is correlated with the O-H impurity concentration, which was determined through FTIR and RBS analyses. The impact of molecular orientation on conductivity anisotropy in organic layers can be studied with the help of wide-angle X-ray diffraction.

There is room for contributions to the modeling of heat conduction in dielectric films, particularly at the atomistic level depicted in Figure 5 and its connection with phonon transport calculations. Atomistic simulations require more precise information about interatomic potentials, which is being established through ab initio calculations (107), as well as a practical approach for handling the quantum-mechanics of vibrational spectra within the lattice. Although a full quantum-mechanical treatment may not be necessary, a modification of the classical force and bond-angle atomistic methodology is needed below the

Debye temperature of the solid. Another approach for improving modeling is to leverage recent advancements in nanofabrication technology to perform fundamental experiments that illuminate the physics of transport. In the past, phonon scattering and wave behavior were studied most extensively at cryogenic temperatures, where the free paths and wavelengths are longest. However, future work must focus on room temperature and above to fully appreciate the impact of phonon dispersion and anharmonic interactions on interfacial scattering and interference. While superlattices and silicon-on-insulator layers provide one vehicle for basic measurements of this type, other types of nanostructures such as silicon nanopillars (108) warrant more attention.

A conspicuous shortcoming of this review is the lack of discussion of several of the most technologically promising materials in Table 1. This results from the absence of data and modeling for these materials and identifies areas where more work is needed. For example, there has been no systematic study on conducting organic films, although the thermal conductivities of these films are strongly process dependent and can govern the peak power output of organic light-emitting diodes and lasers. The thermal conduction properties of a variety of thin-film materials important for wide-bandgap semiconductor devices, including SiC and GaN, have received little attention. There are also relatively few data available for conduction in superlattices, in particular those relevant for solid-state cooling applications. Porous silicon is promising for adsorption-based detectors, thermal insulation in MEMS, and optoelectronic devices. Although there has been some research on the thermal and radiative properties of porous silicon (109–112), more work is needed to determine the dependence on the orientation and volume fraction of pores and the participation of adsorbed species. In summary, there is much room for fruitful research on thermal transport in novel films, which will continue to be motivated by advancements in deposition and growth technology.

ACKNOWLEDGMENTS

Helpful comments and original figures were provided by M Asheghi, K Banerjee, B Chui, T Kenny, K Kurabayashi, Y Leung, M Touzelbaev, and S Wong of Stanford University; G Chen of the University of California, Los Angeles; and R Venkatasubramanium of the Research Triangle Institute. The authors also benefitted from correspondence and discussions with C Scott, IBM Research Institute, Almaden; U Srinivasan and D Fletcher, Stanford University; C Hipwell, Seagate Corporation; J Lukes, University of California, Berkeley; and P Norris, University of Virginia. This work was supported by the Semiconductor Research Corporation through contracts PJ-357 and SJ-461 and by DARPA/ONR through the thermoelectrics program. Additional support was provided by the Office of Naval Research through a Young Investigator Award and NSF through a CAREER Award.

Literature Cited

1. Flöter A, Güttler H, Schulz G, Steinbach D, Lutzelsner C, Zachai R, et al. 1998. *Diamond Rel. Mater.* 7:283–88
2. Deleted in proof
3. Graebner JE. 1993. *Diamond Films Technol.* 4:77–130
4. Touzelbaev MN, Goodson KE. 1998. *Diamond Rel. Mater.* 7:1–14
5. Banerjee K, Amerasekera A, Dixit G, Cheung N, Hu C. 1997. *Proc. Int. Reliability Physics Symp. IEEE* 35983:216–20
6. Venkatasubramanian R, Colpitts T, Watko E, Hutchby J. 1996. *Proc. 15th Int. Conf. Thermoelectrics.* 8169:454–58
7. Hicks LD, Dresselhaus MS. 1993. *Phys. Rev. B* 47:12727–31
8. Leung YK, Kuehne SC, Huang VSK, Nguyen CT, Paul AK, et al. 1997. *Electron Device Lett.* 18:13–15
9. Ju YS, Käding OW, Leung YK, Wong SS, Goodson KE. 1997. *Electron Device Lett.* 18:169–71
10. Chui BW, Stowe TD, Ju YS, Goodson KE, Kenny TW, et al. 1998. *J. Micro Electro Mechanical Syst.* 7:69–78
11. Casimir HBG. 1938. *Physica* 5:495–500
12. Ziman JM. 1960. In *Electrons and Phonons*, pp. 470–82. London: Oxford Univ. Press. 554 pp.
13. Narayanamurti V, Störmer HL, Chin MA, Gossard AC, Wiegmann W. 1979. *Phys. Rev. Lett.* 43:2012–15
14. Ren SY, Dow JD. 1982. *Phys. Rev. B* 25: 3750–55
15. Colvard C, Grant TA, Klein MV, Merlin R, Fischer R, et al. 1985. *Phys. Rev. B* 31: 2080–91
16. Srivastava GP. In *The Physics of Phonons*, pp. 253–85. New York: Hilger. 421 pp.
17. Asheghi M, Leung YK, Wong SS, Goodson KE. 1997. *Appl. Phys. Lett.* 71:1798–1800
18. Asheghi M, Touzelbaev MN, Goodson KE, Leung YK, Wong SS. 1998. *J. Heat Transfer* 120:31–36
19. Ju YS, Goodson KE. 1999. *Appl. Phys. Lett.* In press
20. Goodson KE, Käding OW, Rösler M, Zachai R. 1995. *J. Appl. Phys.* 77:1385–92
21. Verhoeven H, Boettger E, Flöter A, Reiss H, Zachai R. 1997. *Diamond Rel. Mater.* 6:298–302
22. Bauer S, De Reggi AS. 1996. *J. Appl. Phys.* 80:6124–28
23. Rogers JA, Yang Y, Nelson KA. 1994. *Phys. A* 58:523–34
24. Ju YS, Kurabayashi K, Goodson KE. 1999. *Thin Solid Films.* 339:160–64
25. Kurabayashi K, Touzelbaev MN, Asheghi M. 1999. *J. MicroElectroMechanical Syst.* In press
26. Ju YS, Goodson KE. 1999. *J. Appl. Phys.* In press
27. Cahill DG, Fischer HE, Klitsner T, Swartz ET, Pohl RO. 1989. *J. Vacuum Sci. Technol.* A7:1259–66
28. Swartz ET, Pohl RO. 1989. *Rev. Mod. Phys.* 61:605–68
29. Cahill DG. 1997. *Microscale Thermophys. Eng.* 2:85–109
30. Goodson KE, Flik MI. 1994. *Appl. Mech. Rev.* 47:101–12
31. Plamann K, Fournier D. 1995. *Diamond Rel. Mater.* 4:809–19
32. Hyldgaard P, Mahan GD. 1997. *Phys. Rev. B* 56:10754–57
33. Chen G. 1998. *Phys. Rev. B* 57:14958–73
34. Chen G. 1998. *J. Heat Transfer* 119:220–29
35. Ward IM. 1983. *Mechanical Properties of Solid Polymers*. New York: Wiley & Sons
36. Uher CU. 1990. *J. Supercond.* 3:337–89
37. Richardson RA, Peacor SD, Uher C, Nori F. 1992. *J. Appl. Phys.* 72:4788–91
38. Goodson KE, Flik MI. 1993. *J. Heat Transfer* 115:17–25
39. Goodson KE, Flik MI, Su LT, Antoniadis DA. 1993. *Electron Device Lett.* 14:490–92
40. Goodson KE, Flik MI, Su LT, Antoniadis DA. 1994. *J. Heat Transfer* 116:317–24
41. Cahill DG, Katiyar M, Abelson JR. 1994. *Phys. Rev. B* 50:1464–70
42. Zhou SQ, Chen G, Liu JL, Zheng XY, Wang KL. 1998. Presented at *Proc. Int. Mechanical Engineering Congr. Expo. Anaheim, CA.*
43. Cahill DG. 1990. *Rev. Sci. Instruments* 61:802–8
44. Capinski WS, Maris HJ. 1996. *Physica B* 219,220:699–701
45. Morath JC, Maris HJ, Cuomo JJ, Pappas DL, Grill A, et al. 1994. *J. Appl. Phys.* 76:2636–40
46. Hostetler JL, Smith AN, Norris PM. 1997.

Microscale Thermophys. Eng. 1:237–44
47. Käding OW, Skurk H, Goodson KE. 1994. *Appl. Phys. Lett.* 65:1629–31
48. Goodson KE, Käding OW, Rösler M, Zachai R. 1995. *J. Appl. Phys.* 77:1385–92
49. Käding OW, Skurk H, Maznev AA, Matthias E. 1995. *Appl. Phys. A* 61:253–61
50. Käding OW, Matthias E, Zachai R, Fusser HJ, Munziger P. 1993. *Diamond Rel. Mater.* 2:1185–90
51. Wei S, Li C, Chou MY. 1994. *Phys. Rev. B* 50:14587–90
52. Mazzacurati V, Ruocco G, Sampoli M. 1996. *Europhys. Lett.* 34:681–86
53. Li J, Porter L, Yip S. 1998. *J. Nucl. Mater.* 255:139–52
54. Porter LJ, Justo JF, Yip S. 1997. *J. Appl. Phys.* 82:5378–81
55. Stoner RJ, Maris HJ. 1993. *Phys. Rev. B* 48:16373–78
56. Montie EA, van de Walle GFA, Gravesteijn DJ, van Gorkum AA, Teesselink WJO. 1989. *Semicond. Sci. Technol.* 4:889–91
57. Tamura S, Hurley DC, Wolfe JP. 1988. *Phys. Rev. B* 38:1427–49
58. Balandin A, Wang KL. 1998. *Phys. Rev. B* 58:1544–49
59. Tien CL, Chen G. 1994. *J. Heat Transfer* 116:799–807
60. Callaway J. 1959. *Phys. Rev.* 113:1046–51
61. Holland MG. 1963. *Phys. Rev.* 132:2461–71
62. Majumdar A. 1993. *J. Heat Transfer* 115: 7–16
63. Chen G, Tien CL. 1993. *J. Thermophys. Heat Transfer* 7:311–18
64. Goodson KE. 1996. *J. Heat Transfer* 118: 279–86
65. Bardeen J, Rickayzen G, Tewordt L. 1959. *Phys. Rev.* 113:982–94
66. Tewordt L, Wölkhausen Th. 1989. *Solid State Commun.* 70:839–44
67. Peierls RE. 1955. *Quantum Theory of Solids*. New York: Oxford Univ. Press
68. Jagannathan A, Orbach R, Entin-Wohlman O. 1989. *Phys. Rev. B* 39:13465–77
69. Feldman JL, Kluge MD, Allen PN, Wooten F. 1993. *Phys. Rev. B* 48:12589–602
70. Sheng P, Zhou M. 1991. *Science* 253:539–42
71. Cahill DG, Watson SK, Pohl RO. 1992. *Phys. Rev. B* 46:6131–40
72. Fossum JG, Cristoloveanu S, Yoshimi M. 1998. *Trans. Electron Devices* 45:998–99
73. Wilson SR, Wetteroth T, Hong S, Shin H, Hwang BY, et al. 1996. *J. Electron. Mater.* 25:13–21
74. Denton JP, Neudeck GW. 1996. *Electron Device Lett.* 17:509–11
75. Bruel M, Aspar B, Auberton-Herve AJ. 1997. *Jpn. J. Appl. Phys.* 36:1636–41
76. Sondheimer EH. 1952. *Adv. Phys.* 1:1–42
77. Savvides N, Goldsmid HJ. 1974. *Phys. Stat. Solid.* B63:K89–91
78. Sood KC, Roy MK. 1993. *J. Phys.: Condens. Matter* 5:301–12
79. Chen G. 1997. *J. Heat Transfer* 119:220–29
80. Lee SM, Cahill DG, Venkatasubramanian R. 1997. *Appl. Phys. Lett.* 70:2957–59
81. Chen G, Neagu M. 1997. *Appl. Phys. Lett.* 71:2761–63
82. Richards PL. 1994. *J. Appl. Phys.* 76:1–24
83. Prasher RS, Phelan PE. 1997. *J. Supercond.* 10:473–84
84. Crommie MF, Zettl A. 1991. *Phys. Rev. B* 43:408–12
85. Fanton JT, Mitzi DB, Kapitulnik BT, Khuri-Yakun BT, Kino GS, et al. 1989. *Appl. Phys. Lett.* 55:598–99
86. Cohn JL, Wolf SA, Vandera TA. 1992. *Phys. Rev. B* 45:511–14
87. Cohn JL, Wolf SA, Vanderah TA, Selvamanickam V, Salama K. 1992. *Physica C* 192:435–42
88. Ikebe M, Fujishiro H, Naito T, Matsukawa M, Noto K. 1994. *Jpn. J. Appl. Phys.* 33: 6157–59
89. Hagen SJ, Wang ZZ, Ong NP. 1989. *Phys. Rev. B* 40:9389–91
90. Stoner BR, Ma GHM, Wolter SD, Glass JT. 1992. *Phys. Rev. B* 45:11067–84
91. Touzelbaev MN, Goodson KE. 1997. *J. Thermophys. Heat Transfer* 11:506–12
92. Morelli DT, Uher C, Robinson CJ. 1992. *Appl. Phys. Lett.* 62:1085–87
93. Williams BE, Glass JT. 1989. *J. Mater. Res.* 4:373–84
94. Heatherington AV, Wort CJH, Southworth P. 1990. *J. Mater. Res.* 5:1591–94
95. Stiegler J, Lang T, Nygardferguson M, Vonkaenel Y, Blank E. 1996. *Diamond Rel. Mater.* 5:226–30
96. Michler J, Stiegler J, Vonkaenel Y, Moeckli P, Dorsch W, et al. 1997. *J. Cryst. Growth* 172:404–15
97. Cahill DG, Allen TH. 1994. *Appl. Phys. Lett.* 65:309–11
98. Lee SM, Cahill DG. 1997. *J. Appl. Phys.* 81:2590–95
99. Kleiner MB, Kühn SA, Weber W. 1996. *Trans. Electron Devices* 43:1602–9
100. Cahill DG, Tait RH, Stephens RB, Watson SK, Pohl RO. 1990. In *Thermal Conductivity*. 21:3–16. New York: Plenum
101. Einarsrud MA, Haereid S, Wittwer V.

1993. *Solar Energy Mater. Solar Cells*. 31:341–47
102. Nagasima B. 1972. *J. Appl. Phys.* 43: 3378–86
103. Kurabayashi K, Goodson KE. 1998. *Stanford Univ. Rept.* TSD–115
104. Henning J. 1967. *J. Polym. Sci.* C16: 2751–61
105. Kurabayashi K, Goodson KE. 1999. *ASME/JSME Thermal Eng. Conf.* In press
106. Hatta H, Taya M. 1986. *Int. J. Eng. Sci.* 24:1159–72
107. Bazant MZ, Kaxiras E, Justo JF. 1997. *Phys. Rev. B* 56:8542–88
108. Liu HI, Biegelsen DK, Ponce FA, Johnson NM, Pease RFW. 1994. *Appl. Phys. Lett.* 64:1383–85
109. Cruz-Orea A, Delgadillo I, Vargas H, Gudino-Martinez A, Martin E, et al. 1996. *J. Appl. Phys.* 79:8951–54
110. Amato G, Benedetto G, Boarino L, Brunetto N, Spagnolo R. 1997. *Opt. Eng.* 36:423–31
111. Hipwell MC, Tien CL, Mao X, Russo XM. 1998. *Microscale Thermophys. Eng.* 2:87–99
112. Hipwell MC, Tien CL. 1998. *Exp. Heat Transfer* 11:281–97